Variable Temperature Neutron Diffraction and X-Ray Charge Density Studies of Tetraacetylethane

Paula M. B. Piccoli,*,† Thomas F. Koetzle,† Arthur J. Schultz,† Elizabeth A. Zhurova,‡ Jernej Stare,§ A. Alan Pinkerton,‡ Juergen Eckert,|| and Dusan Hadzi§

Intense Pulsed Neutron Source, Argonne National Laboratory, Argonne, Illinois 60439, Department of Chemistry, University of Toledo, Toledo, Ohio 43606, National Institute of Chemistry (KI), Hajdrihova 19, SI-1000, Ljubljana, Slovenia, and Materials Research Laboratory, University of California, Santa Barbara, California 93106

Received: January 9, 2008; Revised Manuscript Received: March 19, 2008

Single crystal neutron diffraction data have been collected on a sample of enolized 3,4-diacetyl-2,5-hexanedione (tetraacetylethane, TAE) at five temperatures between 20 and 298 K to characterize the temperature-dependent behavior of the short, strong, intramolecular hydrogen bond. Upon decreasing the temperature from 298 K to 20 K, the O2−H1 distance decreases from 1.171(11) to 1.081(2) Å and the O1···H1 distance increases from 1.327(10) to 1.416(6) Å. The convergence of the C−O bond lengths from inequivalent distances at low temperature to identical values (1.285(4) Å) at 298 K is consistent with a resonance-assisted hydrogen bond. However, a rigid bond analysis indicates that the structure at 298 K is disordered. The disorder vanishes at lower temperatures. Short intermolecular C−H···O contacts may be responsible for the ordering at low temperature. The intramolecular O···O distance (2.432 ± 0.006 Å) does not change with temperature. X-ray data at 20 K were measured to analyze the charge density and to gain additional insight into the nature of the strong hydrogen bond. Quantum mechanical calculations demonstrate that periodic boundary conditions provide significant enhancement over gas phase models in that superior agreement with the experimental structure is achieved when applying periodicity. One-dimensional potential energy calculations followed by quantum treatment of the proton reproduce the location of the proton nearer to the O2 site reasonably well, although they overestimate the O−H distance at low temperatures. The choice of the single-point energy calculation strategy for the proton potential is justified by the fact that the proton is preferably located nearer to O2 rather than being equally distant to O1 and O2 or evenly distributed (disordered) between them.

Introduction

The short, strong hydrogen bond has been the subject of renewed attention over the past several years, in part because it may be viewed as a model for a purported transition state or an intermediate in enzymatic processes involving proton transfer. Neutron diffraction in particular is an indispensible technique in the characterization of short strong hydrogen bonds.[1–4] In general, a short hydrogen bond may be defined as having a D−H···A distance of 2.7 Å or less. The β-diketone enols are an ideal class of hydrogen bonded compounds for this type of study because their intramolecular hydrogen bond geometry forces the D−H···A distances to be among the shortest known. One possible explanation for the strength of these short hydrogen bonds has been provided by the concept of resonance-assisted hydrogen bonding (Chart 1).[5] The resonance-assisted hydrogen bond (RAHB) model was developed by Gilli and co-workers to explain the correlation between *cis*-enol compounds that possess a high degree of symmetry of the proton transfer equilibrium, a short O−H···O distance, and a lengthening of the covalent O−H bond.

CHART 1

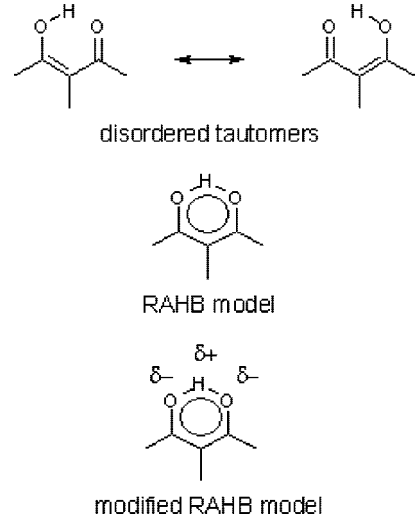

The classic example of a β-diketone enol exhibiting a RAHB is the structure of benzoylacetone[6,7] in which equivalent C−O bond distances, a lack of disorder in the structure and a topological analysis of the electron density revealed a π-delocalization of electrons and high formal charges on the oxygen atoms that contribute strongly to the RAHB model. The hydrogen bond in benzoylacetone is considered to be partially covalent and partially electrostatic, whereas ordinary hydrogen

* Corresponding author email: pmbpiccoli@hotmail.com.
† Argonne National Laboratory.
‡ University of Toledo.
§ National Institute of Chemistry (KI).
|| University of California.

10.1021/jp800204r CCC: $40.75
Published on Web 07/01/2008

TABLE 1: Crystal data and Structure Refinement Parameters for TAE from Neutron Diffraction

temp, K	20(1)	40(1)	70(1)	110(1)	298(1)
formula	$C_{10}H_{14}O_4$	$C_{10}H_{14}O_4$	$C_{10}H_{14}O_4$	$C_{10}H_{14}O_4$	$C_{10}H_{14}O_4$
fw	198.22	198.22	198.22	198.22	198.22
crystal system	orthorhombic	orthorhombic	orthorhombic	orthorhombic	orthorhombic
space group	*Pbcn* (#60)	*Pbcn* (#60)	*Pbcn* (#60)	*Pbcn* (#60)	*Pbcn* (#60)
a, Å	9.066(2)	9.062(1)	9.079(1)	9.083(3)	9.106(2)
b, Å	9.230(2)	9.216(2)	9.247(2)	9.272(3)	9.388(2)
c, Å	11.456(2)	11.411(2)	11.464(2)	11.512(3)	11.814(2)
V, Å^3	958.6(8)	952.9(4)	962.4(3)	969.5(5)	1009.9(4)
Z	4	4	4	4	4
d_{calc}, g cm^{-3}	1.374	1.387	1.368	1.365	1.305
size, mm^3	4 x 4 x 2	4 x 4 x 2	4 x 4 x 2	4 x 4 x 2	4 x 4 x 2
radiation	neutrons	neutrons	neutrons	neutrons	neutrons
data collection technique	time-of-flight Laue	time-of-flight Laue	time-of-flight Laue	time-of-flight Laue	time-of-flight Laue
$\mu(\lambda)$, cm^{-1}	$1.496 + 1.114\lambda$	$1.496 + 1.114\lambda$	$1.496 + 1.114\lambda$	$1.496 + 1.114\lambda$	$1.496 + 1.114\lambda$
max, min transmission	0.5914, 0.1016	0.5914, 0.1016	0.5914, 0.1016	0.5914, 0.1016	0.5914, 0.1016
extinction parameter	$4.8(1) \times 10^{-5}$	$3.34(8) \times 10^{-5}$	$4.5(1) \times 10^{-5}$	$3.5(2) \times 10^{-5}$	$3.4(2) \times 10^{-5}$
d_{min}, Å	0.5	0.5	0.5	0.5	0.7
no. of reflns	3518	4987	3674	1127	1063
no. of reflns ($I > 3\sigma(I)$)[b]	2874	4074	2869	994	805
no. unique reflns ($I > 3\sigma(I)$)[b]	1919	2153	1565	726	537
no. of parameters refined	145	153	147	141	147
refinement method	F^2 [a]	F^2 [a]	F^2 [a]	F^2 [a]	F^2 [a]
R indices $R_w(F^2)$[c], $R(F^2)$[d]	0.096, 0.104	0.096, 0.101	0.095, 0.106	0.079, 0.078	0.087, 0.089
goodness-of-fit	1.46	1.49	1.46	1.70	1.73

[a] Weights were assigned as $w(F_o^2) = 1/[(\sigma(F_o^2) + (0.002F_o^2)]^2$, where $\sigma^2(F_o^2)$ is the variance based on counting statistics. [b] Outliers with $|F_o^2/F_c^2| > 2$, $|F_c^2/F_o^2| > 2$ and $|(F_o^2 - F_c^2)|/\sigma F_o^2 > 6$ were rejected. [c] $R_w(F^2) = \{\Sigma[w(F_o^2 - F_c^2)^2]/\Sigma[w(F_o^2)^2]\}^{1/2}$, where the weights, *w*, are assigned as specified in footnote *a*. [d] $R(F^2) = \Sigma|F_o^2 - F_c^2|/\Sigma|F_o^2|$.

bonds are considered to be primarily electrostatic.[8,9] On the basis of the findings from this study, a modified RAHB was proposed.[6]

Some thirty years ago a room temperature neutron structure of the β-diketone enol tetraacetylethane (TAE) characterized the asymmetric position of the enolic hydrogen atom and equivalent C−O bond distances.[10] A single crystal ^{13}C NMR study from 1986 at room temperature on TAE revealed that the chemical shift tensors of the carbonyl and enolic carbons are different at room temperature. This is in agreement with the difference in the electric field gradient tensors of the respective oxygens observed in the ^{17}O nuclear double resonance spectra.[11] The difference is reduced by increasing temperature. Infrared and Raman spectra of solid TAE and its solution were investigated by Tayyari et al.[12] but the interpretation supported by DFT harmonic frequency calculation is limited to the solutions. Investigation of the vibrational dynamics of solid TAE is ongoing and will be published separately. An X-ray diffraction study of TAE in 2003 found that the hydrogen-bonded proton migrates from a more centrally located position at 298 K to a position closer to the oxygen to which it is covalently bound at 110 K.[13] In an effort to accurately define the geometry of the migrating proton in the very short hydrogen bond (O···O = 2.43 Å), we present here the results of single crystal neutron diffraction studies at five temperatures between 20 and 298 K. We have also obtained the electron density derived from X-ray data at 20 K to characterize the electronic structure in the system and the nature of the short, strong, intramolecular hydrogen bond. The molecular symmetry of TAE offers two important features in the study of its hydrogen bond: (1) the proton is not constrained to lie on a crystallographic symmetry element, and (2) this may be viewed as a proton affinity (PA)/pK_a matched system because the aliphatic substituents are identical, a feature considered to be important in short, strong, and highly symmetric hydrogen bonds often exhibiting covalent character.[14,15] Experimental studies reported in this article are supported by quantum mechanical calculations based both on isolated molecules and on periodic models.

Experimental Methods

General Information. TAE was obtained from Frinton Laboratories, Inc. Single crystals were grown by slow evaporation from an acetone solution.

Neutron Data Collection. Neutron diffraction data were obtained at the Intense Pulsed Neutron Source (IPNS) at Argonne National Laboratory using the time-of-flight Laue single-crystal diffractometer (SCD).[16] At the IPNS, pulses of protons are accelerated into a heavy-element target 30 times a second to produce pulses of neutrons by the spallation process. Exploiting the pulsed nature of the source, neutron wavelengths are determined by time-of-flight on the basis of the de Broglie equation $\lambda = (h/m)(t/l)$, where *h* is Planck's constant, *m* is the neutron mass, and *t* is the time-of-flight for a flight path *l*, so that the entire thermal spectrum of neutrons can be used. With position-sensitive area detectors and a range of neutron wavelengths, a solid volume of reciprocal space is sampled with each stationary orientation of the sample and the detectors. The SCD has two ^{6}Li-glass scintillation position-sensitive area detectors, each with active areas of 15×15 cm^2 and a spatial resolution of <1.5 mm. One of the detectors is centered at a scattering angle of 75° and a crystal-to-detector distance of 23 cm, and the second detector is at 120° and 18 cm. Details of the data collection and analysis procedures have been published previously.[17]

A crystal of $C_{10}H_{14}O_4$ (**1**), with approximate dimensions of $4 \times 2 \times 2$ mm^3, was wrapped in aluminum foil and glued to an aluminum pin that was mounted on the cold stage of a closed-cycle helium refrigerator. The sample was cooled under vacuum to the temperature at which data were collected (see Table 1). The same crystal was used for all five temperatures in this study. For each setting of the diffractometer angles, data were stored in three-dimensional histogram form with coordinates *x*, *y*, *t* corresponding to horizontal and vertical detector positions and the time-of-flight, respectively. An auto-indexing algorithm[18] was used to obtain an initial orientation matrix from the peaks in three preliminary histograms measured for 30 min each. This

TABLE 2: Details for the X-ray Diffraction Experiment

temp, K	20(2)
formula	$C_{10}H_{14}O_4$
fw	198.22
crystal system	orthorhombic
space group	*Pbcn* (#60)
a, Å	9.0859(18)
b, Å	9.2413(18)
c, Å	11.465(2)
V, Å^3	962.7(3)
Z	4
d_{calc}, g cm^{-3}	1.368
size, mm^3	0.25 × 0.25 × 0.20
radiation	Mo Kα (0.71073 Å)
data collection technique	ω-scans
$\mu(\lambda)$, cm^{-1}	0.011
extinction parameter	0.011(3)
θ min, max	3.14, 71.01
no. of reflections	54656
no. of unique reflections	4861
R_{int}/average data multiplicity	0.0241/11.2
no. reflns used ($I > 4\sigma(I)$) measured more than 2 times	3530
no. of parameters refined	268
refinement method	F^2
R indices *R*, *wR*	0.0167, 0.0520
goodness-of-fit	1.1506

unit cell approximately matched the previously reported X-ray unit cell,[13] indicating that the neutron sample was the authentic material. For intensity data collection, runs of 4 hours per histogram were initiated for the 70, 110 and 298 K data sets and 5 hours for the 20 and 40 K data sets. Settings were arranged at χ and ϕ values suitable to cover at least one unique octant of reciprocal space (Laue symmetry *mmm*). With the above counting times, 9 histograms were collected at 20 K, 13 histograms were collected at 40 K, 7 histograms were collected for the 110 K data set and 10 histograms for the 70 and 298 K data sets during the days available for the experiments. The recorded peaks in each histogram were indexed and integrated using individual orientation matrices for each histogram, to allow for any misalignment of the sample. The intensities were corrected for the wavelength dependence of the incident spectrum, the detector efficiency, and the sample absorption (μ (cm^{-1}) = 1.496 + 1.114λ).

Neutron Refinement. A wavelength-dependent spherical absorption correction was applied using cross sections from Sears[19] for the nonhydrogen atoms and from Howard et al.[20] for the hydrogen atoms. Symmetry related reflections were not averaged because different extinction factors are applicable to reflections measured at different wavelengths. The GSAS software package was used for structural analysis.[21] The atomic positions of the X-ray diffraction structure except for H1 were used as a starting point in the refinement. H1 was clearly located in a difference Fourier map during the isotropic stages of refinement. The refinement was based on F^2 with a minimum *d*-spacing of 0.5 Å. Weights were assigned as $w(F_o^2) = 1/[(\sigma(F_o^2) + (0.002F_o^2)]^2$, where $\sigma^2(F_o^2)$ is the variance based on counting statistics. In the final refinement all atoms, including hydrogen atoms, were refined with anisotropic displacement parameters. Data collection and refinement parameters are summarized in Table 1, and selected bond distances and angles in Tables 3 and 4, respectively. The positional and displacement parameters are listed in the accompanying cif files with complete lists of bond lengths and angles. After final refinement, the maximum peak of unmodeled scattering density in the difference Fourier map was 0.269 fm/Å^3 for 20 K, 0.291 fm/Å^3 for 40 K, 0.266 fm/Å^3 for 70 K, 0.127 fm/Å^3 for 110 K and 0.064 fm/Å^3 for 298 K; for each data set these numbers compare to approximately 2−4% of the peak height of carbon atom C1 in a Fourier map. The neutron scattering density of hydrogen is negative, and the residual scattering length density accordingly appears as a "hole" in the difference Fourier map. Refinement on omitting H1 resulted in increased *R*-indices [$wR(F^2) = 0.258$, 20 K; $wR(F^2) = 0.237$, 40 K; $wR(F^2) = 0.225$, 70 K; $wR(F^2) = 0.257$, 110 K; $wR(F^2) = 0.195$, 298 K] and a large negative peak in the difference Fourier map at the position of H1 (−2.380 fm/Å^3, 20 K; −2.844 fm/Å^3, 40 K; −1.669 fm/Å^3, 70 K; −0.862 fm/Å^3, 110 K; −0.347 fm/Å^3, 298 K).

TABLE 3: Intramolecular Bond Distances (Å) for TAE

	20 K	40 K	70 K	110 K	298 K
O1−C1	1.2672(12)	1.2659(9)	1.2647(11)	1.268(3)	1.284(4)
O2−C3	1.3087(12)	1.3086(9)	1.3101(11)	1.310(2)	1.285(4)
C1−C2	1.4399(10)	1.4364(9)	1.4407(13)	1.4320(18)	1.418(3)
C1−C4	1.4932(11)	1.4913(9)	1.4918(13)	1.490(2)	1.489(4)
C2−C2′	1.4876(14)	1.4895(11)	1.4898(13)	1.493(3)	1.490(4)
C2−C3	1.3915(10)	1.3867(9)	1.3912(12)	1.391(2)	1.403(3)
C3−C5	1.4932(11)	1.4897(9)	1.4923(14)	1.491(2)	1.500(4)
H1···O1	1.416(2)	1.411(2)	1.407(3)	1.393(4)	1.327(10)
H1−O2	1.081(2)	1.082(2)	1.091(3)	1.097(4)	1.171(11)
O1···O2	2.434(1)	2.429(1)	2.435(2)	2.426(2)	2.435(6)
H2−C4	1.090(2)	1.0825(18)	1.084(3)	1.072(4)	1.007(10)
H3−C4	1.092(2)	1.0823(17)	1.082(3)	1.090(4)	1.038(8)
H4−C4	1.084(2)	1.0812(19)	1.093(2)	1.094(4)	1.046(13)
H5−C5	1.086(2)	1.0797(17)	1.0845(19)	1.061(5)	1.046(13)
H6−C5	1.083(2)	1.0798(19)	1.075(3)	1.066(5)	0.945(14)
H7−C5	1.095(2)	1.0854(18)	1.097(3)	1.077(4)	1.021(12)

X-ray Data Collection and Refinement. Data on a 0.25 × 0.25 × 0.20 mm^3 single crystal sample of TAE were collected on a Rigaku R-axis Rapid diffractometer with a high power Mo rotating anode generator (18 kW), graphite monochromator, and a curved image plate detector. The crystal was glued to the end of a hollow quartz capillary and mounted directly in a helium cold stream at approximately 20(1) K. To obtain sufficient redundancy of data, three complete runs covering 0−180° in ω were collected at different χ and φ settings, two at $\chi = 0$ ($\varphi = 0$, 180°) and one at $\chi = 45°$ ($\varphi = 0°$). To avoid significant overlap of reflections in any one image, a 6° ω-scan range was chosen. Oscillation ranges for adjacent images overlapped by 3° to provide precise scaling between them. Thus, each run consisted of a total of 59 images. An exposure time of 75 s per image was chosen to maximize scattering power and avoid saturation of the strongest reflections. The measurement was completed in ∼10 h. The collected data were integrated with the program VIIPP[22,23] using the predicted reflection positions from the program *HKL2000*.[24] Reflections below $4\sigma(I)$ were rejected during the integration, as well as partial and overlapped reflections. Data have been corrected for the Lorentz-polarization effect. Effects of absorption ($\mu = 0.011$ cm^{-1}) and thermal diffuse scattering at 20 K were considered to be negligible. Data were scaled and then averaged in the *mmm* point group with the program SORTAV.[25] Most of the scaling factors for different images were very close to unity (usually within 1%, however, in several cases differences of up to 5.5 % were observed). Extreme outliers (12 reflections) were rejected during averaging, and reflections measured no more than twice were also discarded from the final data set. Other experimental details are given in Table 2. Initial refinement of the X-ray structure was carried out using SHELXTL.[26] The X-ray data were then fitted to the aspherical atoms formalism developed by Stewart[27] and Hansen and Coppens.[28] Multipole refinement of the X-ray data was carried out with the program XD.[29]

TABLE 4: Intramolecular Bond Angles (deg) for TAE

	20 K	40 K	70 K	110 K	298 K
C1−O1−H1	101.40(10)	101.43(8)	101.49(10)	101.88(19)	101.9(4)
C3−O2−H1	104.11(12)	104.04(9)	104.17(12)	103.9(2)	103.1(4)
O1−C1−C2	121.39(7)	121.43(6)	121.50(8)	121.33(14)	120.9(2)
O1−C1−C4	117.99(7)	118.08(6)	117.99(9)	118.17(13)	117.5(2)
C2−C1−C4	120.61(7)	120.49(5)	120.50(6)	120.49(13)	121.6(2)
C1−C2−C2′	120.58(6)	120.47(5)	120.47(7)	120.61(12)	120.57(19)
C1−C2−C3	117.60(7)	117.56(5)	117.64(6)	117.50(12)	118.1(2)
C2′−C2-C3	121.83(6)	121.97(5)	121.88(8)	121.89(11)	121.4(2)
O2−C3−C2	121.48(7)	121.56(6)	121.28(9)	121.58(13)	121.7(2)
O2−C3−C5	114.61(7)	114.56(6)	114.69(8)	114.87(14)	114.7(3)
C2−C3−C5	123.91(7)	123.88(5)	124.03(6)	123.55(14)	123.6(3)
O1−H1−O2	153.90(18)	153.85(13)	153.79(15)	153.7(4)	154.2(6)
C1−C4−H2	109.52(13)	109.63(11)	110.00(16)	110.4(2)	111.2(4)
C1−C4−H3	110.08(14)	109.27(11)	109.86(14)	108.5(3)	108.3(5)
C1−C4−H4	111.55(14)	111.58(12)	111.80(17)	111.5(2)	112.0(5)
H2−C4−H3	109.3(2)	110.30(17)	109.8(3)	110.0(4)	112.4(8)
H2−C4−H4	106.6(2)	106.39(16)	105.6(2)	105.8(4)	105.3(8)
H3−C4−H4	109.7(2)	109.64(17)	109.7(2)	110.6(4)	107.6(7)
C3−C5−H5	112.54(13)	112.32(11)	112.41(17)	113.0(2)	113.3(4)
C3−C5−H6	109.92(14)	109.81(11)	110.10(17)	109.5(3)	110.9(6)
C3−C5−H7	109.03(14)	109.04(12)	108.49(19)	109.2(3)	108.5(7)
H5−C5−H6	109.3(2)	109.84(18)	109.7(3)	110.0(4)	112.6(10)
H5−C5−H7	108.9(2)	108.68(17)	108.9(2)	107.7(5)	101.9(11)
H6−C5−H7	107.0(2)	107.00(19)	107.2(3)	107.3(5)	109.1(11)

The hydrogen atoms were fixed at the positions determined from the 20 K neutron structure. Anisotropic displacement parameters of the non-hydrogen atoms were determined from the X-ray refinement; the anisotropic displacement parameters of the hydrogen atoms from the neutron data were scaled appropriately to match the anisotropic displacement parameters from the X-ray refinement and were subsequently fixed at these values during the multipole refinement. Oxygen atoms were refined to the hexadecapole level, and carbon atoms to the octapole level, whereas hydrogen atoms were truncated at the quadrupole level. Refining κ' values for the multipoles of the hydrogen atoms did not give reasonable results; therefore a theoretical calculation of the TAE crystal with the experimental geometry (DFT B3LYP/6-31G** with the CRYSTAL98 package[30]) followed by a multipole refinement ($R = 0.0050$) was performed. Then, the κ'(H) values for the experimental data were fixed at the theoretical values (1.294(9)). All initial chemical constraints were released in the final refinement.

Computational Details. Gas phase calculations (isolated TAE molecule) were performed using the Gaussian 03 program package[31] using the B3LYP/6-31+G(d,p) level of theory, and calculations on the periodic crystalline model were carried out by the CPMD program package.[32] The periodic model was built on the basis of the X-ray diffraction data at 20 K (see Table 2), taking into account all symmetry elements that originate from the *Pbcn* space group. The electronic structure in the solid was calculated with the BLYP density functional; a plane wave basis set with a kinetic energy cutoff of 25 Ry together with the Vanderbilt ultrasoft atomic pseudopotentials[33] has been used. Geometry optimization in the solid was performed under the constraint of frozen unit cell parameters. At the first stage, geometry optimization was performed with both the isolated and the crystal model. Consistency of geometry optimization was ensured by harmonic frequency checks.

Next, a one-dimensional proton potential along the O−H line was constructed with both models by displacing the H-bonded proton from r(OH) = 0.75 Å to 1.80 Å in 0.05 Å steps and keeping the other nuclei frozen in their optimized positions (single point potential energy scan). Although this is likely to be a rough approximation of the actual proton motion, the single point scan has proven to more reliably reproduce certain properties of the H-bond, such as geometric parameters and vibrational frequencies,[34,35] than a relaxed potential energy scan. Having acquired the potential energy function, the vibrational Schrödinger equation was solved for the O−H stretching motion in the given potential by using the variational Fourier Grid Hamiltonian method[36] tuned for the application in generalized internal coordinates,[37] yielding anharmonic vibrational energies and wavefunctions associated with the proton motion along the O−H line. The impact of anharmonicity and quantized proton motion on the O−H distance was determined by calculating the ground state expectation value of r(OH).

Discussion

Description of the Neutron Structure. The molecular structure and labeling scheme of TAE is shown in Figures 1 and 2. With the exception of the anisotropic displacement parameters, which increase with increasing temperature, the overall molecular structure at each of the five temperatures is identical. Interest in the neutron structure of TAE involves the temperature dependent geometry of the short, intramolecular hydrogen bond. Intramolecular bond distances and angles for the five temperatures of the study are listed in Tables 3 and 4, respectively. Gross molecular parameters between 20 K and 110 K vary little within statistical error and can be considered to be equivalent for the purposes of this discussion. Figure 3 shows the change in parameters for the relevant portion of the short hydrogen bond, namely the C−O and O−H···O distances. On decreasing the temperature from 298 K to 20 K, the O2−H1 distance decreases from 1.171(11) to 1.081(2) Å and the O1···H1 distance increases from 1.327(10) to 1.416(6) Å. At any temperature it appears that H1 is more strongly bound to O2, and there is a clear temperature dependence on the atomic position of H1. The long axis of the H1 anisotropic displacement ellipsoid lies along the O1···O2 bond, as is typical for compounds containing a short, strong hydrogen bond.[38] The O1···O2 distance varies little with temperature (vide infra).

The corresponding C−O distances also change significantly on cooling: the O2−C3 distance increases from 1.285(4) to

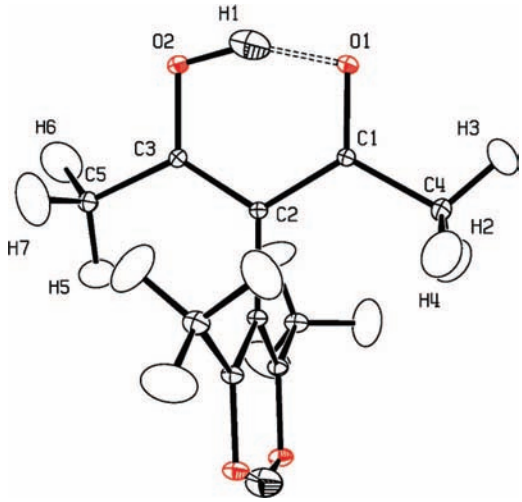

Figure 1. ORTEP of TAE at 20 K showing the hydrogen bond as a dashed, hollow bond. The asymmetric unit is labeled. The two halves of the molecule are related by a crystallographic 2-fold axis bisecting the C2−C2′ bond and oriented at 45° to the plane of the figure. Displacement ellipsoids are plotted at 50% probability.

1.309(1) Å, and the O1−C1 distance decreases from 1.284(4) to 1.267(1) Å. The convergence of the C−O bond lengths to identical values at 298 K (see Figure 3) can be viewed as being consistent with a resonance assisted hydrogen bond description.[5,13] The changes in the C2−C1 and C2−C3 distances from a localized model at 20 K (C2−C1 = 1.440(1) Å, C2−C3 = 1.391(1) Å) to a more delocalized model at room temperature (C2−C1 = 1.418(3) Å, C2−C3 = 1.403(3) Å,) are also consistent with this bonding model. However, it appears that the C2−C1 and C2−C3 distances do not converge at room temperature unlike the case for the C−O distances, although this observation is just barely statistically significant (Δ= 0.015(4) Å). It is likely that a small amount of delocalization persists, which accounts for the intermediate bond lengths at 20 K (typical values: C−C ≈ 1.48, C═C ≈ 1.33, C−O ≈ 1.37, C═O ≈ 1.20 Å), but not to such a large degree as seen in benzoylacetone, even though the hydrogen bond distance is quite short.[6] It is apparent that in TAE, some degree of asymmetry in the short hydrogen bond persists even at higher temperatures unlike in the case of benzoylacetone. In 2006, Lyssenko and Antipin reported that heating TAE to 350 K results in a virtual equalization of the C−C bond lengths in the ring, implying complete delocalization; however, there was no mention of the proton position for the higher temperature structure.[39]

Application of the Hirschfeld rigid bond test[40,41] to the analysis of anisotropic displacement ellipsoids (ADPs) of pairs of bonded atoms reveals that the "delocalized" neutron structure at 298 K fails to meet the requirements of the test ($\Delta\langle u^2\rangle_{AB} <$ 0.0010 Å^2), which indicates that the structure is disordered at this temperature. At 110 K and lower, the structures pass the Hirschfeld rigid bond test, and the disorder vanishes.

Omission of the enolic H1 proton from the refinement of the structure at 298 K results in one large, broad minimum peak in the Fourier difference map (see Figure 4). Any disorder of the proton present due to the dynamic disorder is not visually evident in the map. The shape of the H1 density may be understood by assuming that the hydrogen atom resides predominantly in a single, broad, shallow potential well instead of a double potential well. Modeling the hydrogen bonded proton over two disordered sites at 298 K, starting with O−H distances of roughly 1.08 Å, gave slightly higher R_w values (0.089 versus 0.087) and is not an improvement over the current model. In addition, the partial hydrogen atom bound to O1 refined away from its initially placed position and toward O2.

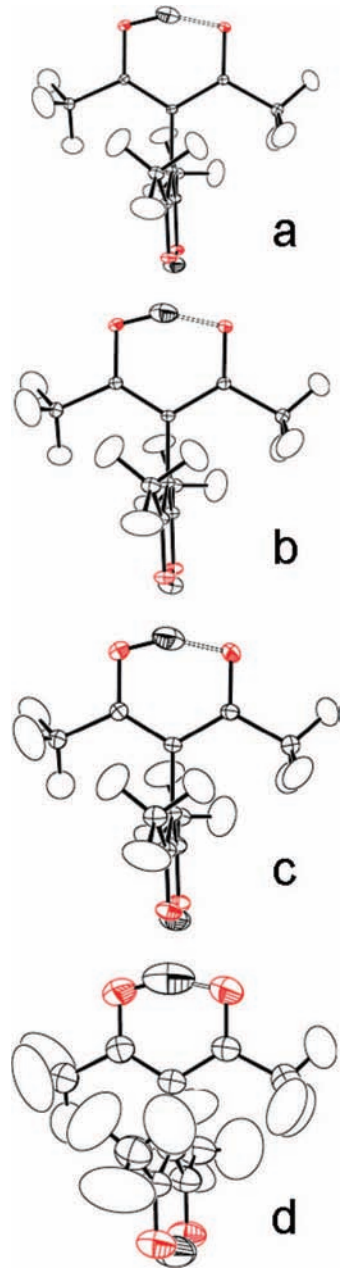

Figure 2. Single crystal neutron structure of TAE at (a) 40 K, (b) 70 K, (c) 110 K and (d) 298 K with numbering scheme the same as in Figure 1. Displacement ellipsoids are plotted at 50% probability.

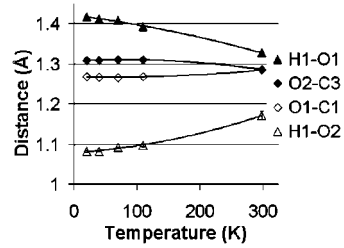

Figure 3. Plot of bond distance (Å) vs temperature (K) for the portions of TAE involving the hydrogen bond. Trend lines added for visual emphasis.

In the 2003 X-ray diffraction study of the compound, it was proposed that a strong *intermolecular* C−H···O interaction on one side of the O···H−O hydrogen bond is responsible for the

TABLE 5: Selected Intermolecular Sub van der Waals O···H Contacts (Å)

	20 K	40 K	70 K	110 K	298 K
O1···H4*	2.496(2)	2.490(2)	2.497(2)	2.511(4)	2.627(9)
O1···H5*	2.679(2)	2.684(2)	2.696(2)	2.733(5)	2.856(1)
O2···H2*	2.293(2)	2.292(2)	2.304(2)	2.316(4)	2.432(9)

removal of the dynamic disorder at low temperature.[13] Table 5 and Figure 5 in the present work indeed detail three such intermolecular interactions with C−H···O distances determined by neutron diffraction to be at or below the sum of the van der Waals radii[42] of 2.72 Å for hydrogen and oxygen at low temperature. An examination of the Hirshfeld surface[43,44] of TAE in Figure 6 highlights the three close contacts in three-dimensional space. The Hirshfeld surface mirrors the results obtained from neutron diffraction and plotted in Figure 5, namely, that the three contacts have interactions of varying intensity, from the O1···H5* contract with the weakest interaction to the O2···H2* contact with the strongest interaction. As reflected in the contraction of the unit cell parameters listed in Table 1, on decreasing the temperature the C−H···O contacts also become shorter. This contraction is related to the reduction in amplitude of low-frequency modes, in particular CH_3 torsions (see Figure 2). It is, however, difficult to separate the contributions of the intermolecular contacts from anharmonic effects on the position of the proton in the hydrogen bond. For the shortest intermolecular interaction one could possibly argue that a closer approach of the more electropositive C4−H2 group to the more electronegative O2 atom draws the H1 hydrogen atom closer to it as well, and the corresponding H1···O1 portion of the hydrogen bond is thereby lengthened. At 20 K, the O2−H1 distance is 1.081(2) Å, still notably longer than the average single O−H bond (from neutron diffraction) of 0.980 Å.[45]

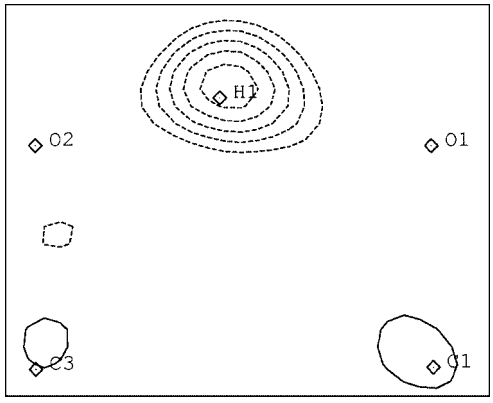

Figure 4. Difference Fourier plot of TAE in the plane of the molecule showing the location of H1 at 298 K. Atom H1 is indicated on the plot but was omitted from the structure factor calculation. The contour intervals are plotted at 0.1 fm/Å^3 in the negative region and 0.50 fm/Å^3 in the positive region; dashed contours indicate negative values.

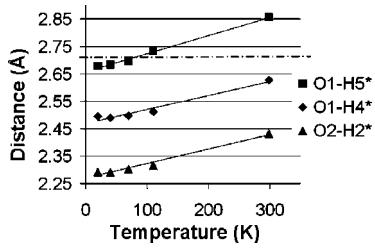

Figure 5. Plot of distance (Å) vs temperature (K) for sub van der Waals contacts between O atoms of TAE and neighboring molecules. The dashed line indicates the van der Waals sum of O and H radii (2.72 Å). Trend lines added for visual emphasis.

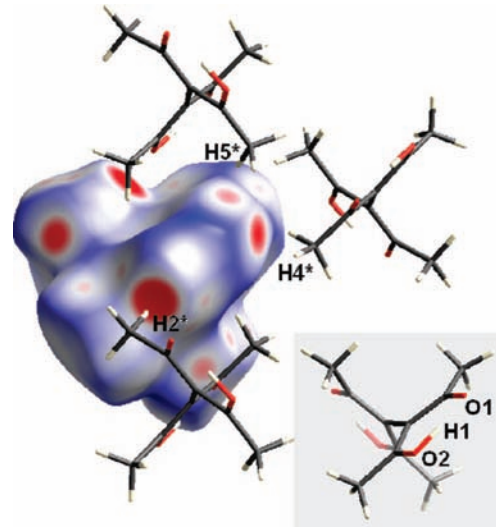

Figure 6. Hirshfeld surface plot of TAE at 20 K showing sub van der Waals intermolecular contacts between neighboring molecules. Large, red areas highlight the close C−H···O donor/acceptor contacts. The inset at the lower right shows the orientation of the TAE molecule inside of the Hirshfeld surface. The Hirshfeld plot was created using CrystalExplorer.[46]

Although the covalent O−H bond distance decreases with decreasing temperature, the intramolecular O1···O2 distance (Table 3) does not change appreciably over the temperature range and, in fact, oscillates about an average value of 2.432(4) Å. The decrease in the O−H distance is accompanied by an apparent equalization of the O1−C1−C2 and O2−C3−C2 bond angles to mean values of 121.39(7)° and 121.48(7)°, respectively (see Table 4). The statistically marginal increase ($\Delta = 0.49(21)°$) in the O1−C1−C2 bond angle between 298 and 110 K may possibly be rationalized by the encroaching C5*−H5*···O1 intermolecular contact: as this interaction increases in strength and shortens to van der Waals contact distance, the bond angle is widened from the effect of pulling the electronegative oxygen atom toward the more electropositive hydrogen atom.

An additional example of a symmetric molecule exhibiting a very short (O···O = 2.391(3) Å) yet asymmetric hydrogen bond at low temperature (15 K) is found in nitromalonamide,[47] whose crystal structure also reveals extensive three-dimensional N−H···O bonding contacts. In fact, the corresponding computational study finds the difference between the symmetric and asymmetric hydrogen bond in nitromalonamide to be about 1 kJ/mol, and the intermolecular hydrogen bonds are invoked to explain the structural difference in similar fashion to the present case.

In TAE it is also interesting to note the slight increase in two of the intermolecular C−H···O distances between 40 and 20 K, which is also reflected in an increase in lattice parameters and cell volume between these two temperatures. It is currently unclear if this is the result of an actual negative thermal expansion of the material in this temperature region or if it is merely an artifact.

X-ray Charge Density and Topological Analysis. The utility of the topological analysis of the electron density has been established in the literature for some time.[48] A plot of the TAE asymmetric unit including the positions of the critical points (CPs) as found in the total electron density is shown in Figure 7. The plot of the model deformation electron density of TAE is shown in Figure 8.

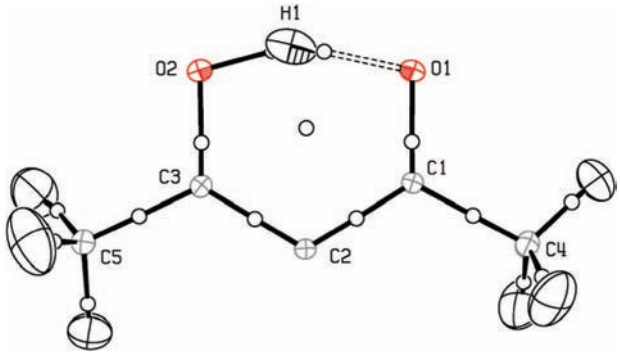

Figure 7. Plot of the asymmetric unit of TAE at 20 K showing critical points (small open circles). The (3, +1) critical point found at the center of the hydrogen bonded six-membered ring is a feature commonly found in ring systems. (3, −1) critical points are located along the bond paths.

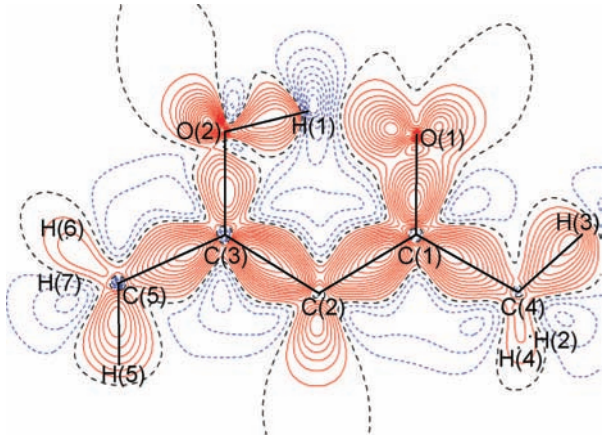

Figure 8. Model deformation electron density of the TAE asymmetric unit. Contours plotted at 0.05 e/Å^3. Solid red lines are positive contours, blue dotted lines are negative contours; the dashed black line is the zero level contour.

The electron density results from the X-ray study at 20 K confirm what is inferred from the bond lengths determined by neutron diffraction: namely that more electron density is located in the O1−C1 carbonyl bond than in the O2−C3 bond. Table 6 gives the results of the topological analysis for the intramolecular interactions. The table lists the experimental ρ_b values for O1−C1 of 2.545 e/Å^3 and O2−C3 of 2.225 e/Å^3, which illustrates the increased amount of electron density at the critical point present in the C═O bond possessing somewhat more formal double-bond character. The C1−C2 and C2−C3 bonds, with ρ_b values of 1.924 and 2.127 e/Å^3, respectively, also confirm that the electron density of the hydrogen bonded six-membered ring is not completely delocalized. Ellipticity values (ϵ, indicating deviation from cylindrical bond symmetry at the CP; we expect that for a completely symmetric sigma-type bond $\epsilon = 0$) for these bonds (0.260 and 0.318, respectively) also indicate that more π-bonding density is found in the shorter of the two C−C bonds.

The hydrogen bond is also found to be asymmetric in terms of its shared electron density, with a O2−H1 ρ_b at the CP of 1.697 e/Å^3 and a H1···O1 ρ_b of 0.681 e/Å^3, less than half that of the covalent bond. The large magnitude of the Laplacian, $\nabla^2\rho_b$, for O2−H1 (−43.99 e/Å^5) shows that the proton is strongly bound to O2. The negative $\nabla^2\rho_b$ value for O1···H1 (−3.27 e/Å^5) classifies the interaction to be a shared shell (or partially covalent) interaction[1] and is typical for both covalent bonds and polar bonds.[49] [Although the theoretical calculation resulted in the positive Laplacian at the O1···H1 CP, the negative value of the electronic energy density (−0.0626 au) and the ratio between the potential and kinetic energy densities at the CP $|V_r|/G_r > 2$ point toward the shared character of this interaction.] The presence of this (3, −1) CP with a negative Laplacian value in the present (20 K) study is in sharp contrast to the topological analysis of Lyssenko's reported charge density of TAE at 110 K, which reports a *positive* Laplacian for the O1···H1 interaction (8.44 e/Å^5).[13] It should be noted that in the 2003 X-ray study, the O−H distance of 1.015 Å was obtained by means of the DFT B3LYP/6-31G** calculation. This value is in fact notably shorter than our experimental neutron result at 20 K and therefore H1 would not have as close an approach to O1; for this reason the topology of the electron density may differ from what we observe at 20 K. The hydrogen bonded six-membered ring in TAE is also characterized by a (3, +1) CP at the center of the ring, a feature commonly found in ring systems, and required to satisfy the Poincaré−Hopf[48] relationship.[50]

A search for bond paths and bond critical points between neighboring molecules in the crystal was performed to characterize the short C−H···O contacts that are implicated in the ordering of the hydrogen bond moiety at low temperature. Apart from the three short C−H···O contacts identified from the neutron parameters, a number of other intermolecular contacts were found, and confirmed by the presence of a virial path.[51] The details of the CPs along these bond paths and their energetics are listed in Table 7. The positive values of the Laplacians and the values of $0 < |V_r|/G_r < 1$, fall into the category of closed shell interactions with no indication of incipient covalent bond formation.[49,52] It is of interest to note that the O2···H2* interaction, the shortest of the three contacts measuring less than the sum of the van der Waals radii (see Figure 5), has the largest ρ_b value (0.062 e/Å^3), and that the O1···H5* interaction, which is the longest of the three, has the lowest ρ_b value (0.020 e/Å^3) of these three short contacts. The additional intermolecular contacts with bond paths and virial paths (outside of the three short C−H···O contacts described above) range from 0.014−0.028 e/Å^3. The previous topological analysis of the charge density of TAE at 110 K[13] reports a (3, −1) CP of one of the short C−H···O contacts as having a ρ_b of 0.04 e/Å^3 but does not report values for any other contacts. This result is less than what we observe for TAE for the shortest contact at 20 K. However, as the neutron data clearly show, the contacts become shorter at low temperature. We therefore expect the interaction to be stronger at 20 K than at 110 K.

Comparison of TAE with Benzoylacetone and Citrinin. Benzoylacetone[6,7] and citrinin[53] are other molecules that exhibit short, strong, intramolecular hydrogen bonds (O···O = 2.50 Å for benzoylacetone; 2.47 and 2.53 Å for citrinin) with the expected configuration for a RAHB.

The large negative value of $\nabla^2\rho_b$ for O2−H1 in TAE is reminiscent of the covalent O−H bonds found in citrinin at 19 K (−49.8 and −33.4 e/Å^5); however, the O···H bonds in citrinin are considered to be closed shell interactions as their $\nabla^2\rho_b$ values are positive (2.25 and 0.10).[53] The covalent O−H distances in citrinin are also less than those found in TAE (1.056(10), 0.974(11) Å), and in this case the positions of the hydrogen atoms were allowed to refine with calculated ADPs. The magnitude of the negative Laplacian for the O1···H1 bond in TAE more closely matches that found for benzoylacetone, whose nearly symmetric hydrogen bond possesses a shared (covalent) interaction.

TABLE 6: (3, −1) Intramolecular Critical Points in the Static Electron Density[a]

bond	ρ_b	$\nabla^2\rho_b$	R_{ij}	d_1	d_2	λ_1	λ_2	λ_3	ϵ
O1−C1	2.545	−29.73	1.271	0.799	0.471	−22.730	−21.092	14.097	0.078
	2.489	−23.42	1.271	0.824	0.446	−20.054	−19.244	15.879	0.042
O2−C3	2.225	−22.97	1.315	0.814	0.501	−18.480	−17.331	12.839	0.066
	2.238	−23.05	1.315	0.832	0.483	−17.090	−16.327	10.370	0.047
C1−C2	1.924	−15.12	1.443	0.756	0.687	−14.970	−11.878	11.726	0.260
	1.946	−15.31	1.443	0.758	0.685	−14.189	−11.413	10.288	0.243
C1−C4	1.733	−12.47	1.495	0.787	0.708	−12.398	−10.982	10.908	0.129
	1.750	−11.94	1.495	0.795	0.700	−11.846	−11.027	10.932	0.074
C2−C2*	1.685	−10.12	1.492	0.746	0.746	−11.591	−11.217	12.685	0.033
	1.671	−9.35	1.492	0.746	0.746	−10.583	−10.555	11.793	0.003
C2−C3	2.127	−18.68	1.394	0.675	0.719	−17.169	−13.024	11.516	0.318
	2.122	−18.59	1.394	0.645	0.749	−15.975	−12.044	9.432	0.326
C3−C5	1.739	−12.77	1.494	0.785	0.709	−12.470	−11.138	10.840	0.120
	1.749	−11.98	1.494	0.793	0.700	−11.938	−10.959	10.918	0.089
O2−H1	1.697	−43.99	1.081	0.858	0.223	−30.447	−28.477	14.930	0.069
	1.793	−29.04	1.081	0.821	0.260	−26.574	−26.037	23.570	0.021
O1···H1	0.681	−3.72	1.420	1.035	0.386	−6.982	−6.568	9.831	0.063
	0.692	0.50	1.420	0.988	0.432	−6.078	−5.965	12.544	0.019
C4−H2	1.826	−18.38	1.090	0.658	0.432	−15.875	−14.963	12.454	0.061
	1.847	−18.81	1.090	0.683	0.407	−16.402	−16.186	13.780	0.013
C4−H3	1.706	−14.80	1.092	0.719	0.373	−15.634	−14.586	15.419	0.072
	1.827	−17.65	1.092	0.682	0.411	−15.959	−15.887	14.196	0.005
C4−H4	1.688	−14.35	1.084	0.688	0.397	−15.018	−13.620	14.288	0.103
	1.857	−18.68	1.084	0.676	0.408	−16.492	−16.107	13.914	0.024
C5−H5	1.632	−13.84	1.086	0.752	0.334	−15.693	−14.415	16.272	0.089
	1.869	−18.95	1.086	0.682	0.404	−16.662	−16.499	14.213	0.010
C5−H6	1.750	−15.15	1.083	0.664	0.419	−15.296	−13.708	13.853	0.116
	1.867	−18.77	1.083	0.675	0.408	−16.484	−16.296	14.006	0.012
C5−H7	1.855	−18.17	1.095	0.628	0.468	−15.225	−14.432	11.488	0.055
	1.798	−17.39	1.095	0.685	0.410	−15.750	−15.515	13.875	0.015

[a] ρ_b (e/Å^3) is the electron density and $\nabla^2\rho_b$ (e/Å^5) is the Laplacian at the CP. $R_{ij} = d_1 + d_2$, where d_1 and d_2 are the distances from the respective atoms to the CP in Å. λ_1, λ_2 and λ_3 are the eigenvalues of the Hessian matrix (e/Å^5). The first line of each entry details results from the analysis of the experimental charge density; the second line of each entry details results from theoretical calculations.

TABLE 7: Topological and Energetic Properties of ρ Calculated at the (3, −1) Critical Points of Intermolecular Interactions[a]

bond	ρ_b	$\nabla^2\rho_b$	R_{ij}	λ_1	λ_2	λ_3	G_r	V_r	$\lvert V_r\rvert/G_r$	H_r
O2···H2*	0.062	0.880	2.296	−0.327	−0.257	1.463	0.007227	−0.00534	0.7386	0.001889
	0.093	0.900	2.296	−0.406	−0.399	1.708	0.008502	−0.00764	0.8985	0.000863
O1···H4*	0.028	0.780	2.501	−0.119	−0.064	0.595	0.005686	−0.00332	0.5832	0.002370
	0.057	0.640	2.501	−0.217	−0.206	1.066	0.005452	−0.00423	0.7766	0.001218
O1···H5*	0.020	0.390	2.685	−0.065	−0.059	0.509	0.002832	−0.00167	0.5890	0.001163
	0.040	0.420	2.685	−0.136	−0.129	0.688	0.003476	−0.00256	0.7376	0.000912
O1···H6*	0.028	0.370	2.974	−0.077	−0.035	0.478	0.002833	−0.00187	0.6597	0.000964
	0.023	0.400	2.974	−0.047	−0.019	0.467	0.003004	−0.00184	0.6128	0.001162
O2···H6*	0.027	0.340	2.903	−0.077	−0.051	0.468	0.002649	−0.00177	0.6678	0.000881
	0.030	0.320	2.903	−0.083	−0.036	0.443	0.002577	−0.00179	0.6962	0.000783
O2···H2*	0.025	0.510	2.779	−0.073	−0.023	0.604	0.003772	−0.00228	0.6042	0.001493
	0.030	0.540	2.779	−0.081	−0.040	0.663	0.004099	−0.00257	0.6270	0.001529
O2···H3*	0.023	0.340	2.779	−0.082	−0.072	0.492	0.002554	−0.00160	0.6257	0.009560
	0.032	0.380	2.779	−0.103	−0.092	0.574	0.003013	−0.00210	0.6953	0.000918
O2···O2*	0.021	0.320	3.313	−0.050	−0.048	0.422	0.002428	−0.00149	0.6149	0.000935
	0.023	0.360	3.313	−0.043	−0.043	0.446	0.002704	−0.00168	0.6202	−0.001800
H2···C4*	0.021	0.450	3.264	−0.079	−0.023	0.556	0.003334	−0.00195	0.5852	0.001382
	0.029	0.510	3.264	−0.094	−0.012	0.615	0.003852	−0.00242	0.6285	0.001435
H3···H7*	0.014	0.230	2.451	−0.053	−0.031	0.309	0.001653	−0.00097	0.5880	0.000681
	0.028	0.360	2.451	−0.097	−0.052	0.505	0.002771	−0.00185	0.6680	0.000920

[a] The first three entries specify the short intermolecular C−H···O contacts that influence the ordering of TAE at low temperature. G_r, V_r and H_r are kinetic, potential and total electronic energy densities at the critical point. Units as in Table 6, except for G_r, V_r and H_r, which are in au. The first line of each entry details results from the analysis of the experimental charge density; the second line of each entry details results from theoretical calculations.

The ellipticities of the C3−O2−H1···O1−C1 portion of the six membered ring range between 0.063 (O1···H1) and 0.078 (O1−C1). The largest of these values occurs for the O1−C1 bond, which is expected from the bond lengths to possess the most π-bonding density. Corresponding ellipticity values for the same ring fragment in benzoylacetone range from 0.10−0.21, which shows greater π-bonding density than is found in the analysis of TAE. This may also be an indicator of the more extensive π-delocalization in benzoylacetone than in TAE. As in TAE, the highest value of the ellipticity corresponds to the shorter of the C−O bonds. The low values of the ellipticities allow us to characterize these bonds as having cylindrical symmetries similar to σ-bonds (contrast this with the large ellipticities in the C−C bonds within the ring, and also those

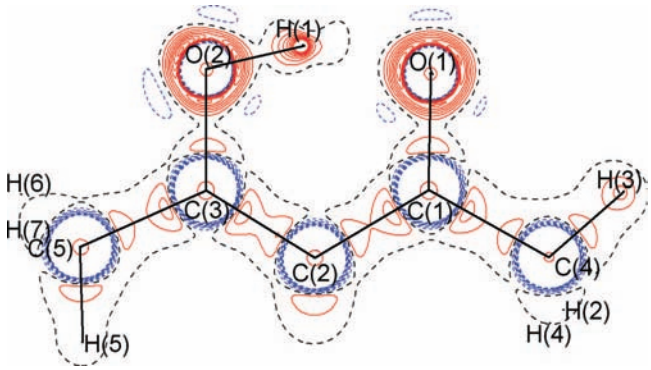

Figure 9. Contour plot of the Laplacian of the electron density, with contours plotted at 15 e/Å^5. Negative (red) values between atomic positions reflect an accumulation of charge density and indicate a shared interaction, including the interaction between oxygen atom O2 and the enolic proton. Lone pairs on oxygen atoms are clearly shown. Note that an area of zero density (dashed black line) surrounds the hydrogen-bonded proton, indicating that the VSCC of H1 is separate from O1.

TABLE 8: Calculated and Experimental H-Bond Geometric Parameters of TAE

model/method	r(O···O) [Å]	r(OH) [Å]	r(O···H) [Å]
gas phase	2.468	1.021 (1.059)[a]	1.525
crystal	2.438	1.070 (1.151)[a]	1.428
experiment (ND, 20 K)	2.434	1.081	1.416
experiment (ND, 298 K)	2.435	1.171	1.327

[a] Values in parentheses correspond to the quantum expectation value of r(OH) over the ground vibrational level (see Figure 10).

found in the benzene portion of benzoylacetone, which indicate significant π-type character).

The O−H···O electron density at the CPs in benzoylacetone is less disparate (0.76(3) and 0.89(3) e/Å^3), as is the density in the C−O bonds (2.54(8) and 2.44(8) e/Å^3) and C−C bonds of the six membered ring (2.04(4) and 2.17(4) e/Å^3), even at very low temperature.[6] The findings from benzoylacetone support a clear case for a completely delocalized RAHB at low temperature, both from the neutron structure and from the charge density study. Results from TAE show that the valence shell charge concentration (VSCC) of the hydrogen-bonded proton is separated from the oxygens (see Figure 9) as in benzoylacetone; this is an indicator that the hydrogen bond has an electrostatic contribution as well,[6,9] even though the topological analysis reveals it to be partially covalent.

Comparison with Computation and the Potential Energy Surface. Table 8 lists the geometric parameters of the H-bond of TAE calculated for the isolated molecule and the periodic system. The periodic model yields shorter O···O (by 0.030 Å) and O···H (by 0.097 Å) distances, but slightly longer O−H distances (by 0.049 Å) than the isolated molecule model. The crystal calculation appears to give a better match with the experimental structure than the isolated one; indeed, the optimized geometric parameters calculated with the periodic model are in a remarkable agreement with the neutron diffraction structure at 20 K. The gas phase model appears to underestimate the strength of the hydrogen bond by all the metric criteria: the O−H distance is too short and the O···O and O···H distances are too long, which clearly points to the importance of intermolecular interactions even for an intramolecular hydrogen bond. Our results agree fairly well with the previous work of others[54] and of two of us[35] in that the medium effect, be it solvent or crystal field, can have a notable impact on the structure and characteristics such as the proton potential functions of H-bonded systems.

A quantum treatment of the proton motion (a calculation based on the one-dimensional potential energy function) increases the expectation value of the O−H distance for both models, whereby the increase is found to be much larger with the crystal model (by 0.081 Å, see Table 8) than with the gas phase model (by 0.038 Å). As these expectation values were obtained from the ground state wavefunctions at 0 K, the value of 1.151 Å calculated with the crystal model (Figure 10) overestimates the experimental low-temperature O−H distance of 1.081 Å, and in fact is closer to the room temperature experimental O−H distance of 1.171 Å. The same treatment based on the gas phase model provides a somewhat better estimate of 1.059 Å, although it is slightly too short. As the energy gap between ground and first excited vibrational level of the proton (Figure 10) is about 4 kcal/mol (~6.7 k_BT at room temperature) for the crystal model and about 6 kcal/mol (~10 k_BT) for the isolated model, excited vibrational levels do not contribute a notable amount to the expectation values, because their Boltzmann factors are too small. The present model based on a one-dimensional proton potential energy function is therefore insufficient for accounting for the observed temperature effect on the geometry of the hydrogen bond. A multidimensional model involving shallow potential energy profiles (e.g., the O···O distance) with thermally accessible excited levels would be essential to overcome the drawback of the model used in this study.

Another approach to reproducing the observed temperature effects, as well as to account for the possible disorder between the proton transfer isomers, would be to perform a set of molecular dynamics (MD) simulations at various temperatures, provided that the simulation time is long enough to cover the phase space for both equilibrium structures. Approaches based on MD simulations that account for proton dynamics in the solid state offer important enhancements in our understanding of the structure and various phenomena, including the phonon effects[55] and the broadening of protonic bands.[56] For that reason we have tentatively performed short molecular dynamics (MD) simulations at various temperatures. We followed the approach published by Morrison and coworkers on the related example of the phosphoric acid-urea complex[57] and carried out simulations at 20, 40, 70, 110 and 298 K; the simulated time was about 1 ps for each of them and the simulations were performed according to the Car−Parrinello scheme. Average values of the O···O, O−H and O···H distances acquired at various temperatures were compared. In agreement with the experiment, the proton exhibited the tendency to migrate towards the center of the H-bond with the increasing temperature, whereas the O···O distance was nearly insensitive to temperature. Nevertheless, we believe for various reasons that this approach together with its results is of a very limited value in the present case. TAE differs considerably from the system studied by Morrison and coworkers in the sense that the TAE molecule is chemically symmetric whereas the phosphoric acid−urea complex is not; the latter features a strongly asymmetric single well potential in various environments.[54,57] Thus it is not surprising that occasional proton jumps from O2 to O1 have been observed in our dynamics simulations, even at 70 K, but not at 20 or 40 K. This results in the necessity to perform sufficiently long MD simulations (probably some tens of picoseconds) to effectively sample the relevant phase space which includes a substantial set of structures with the proton nearer to either the O1 or the

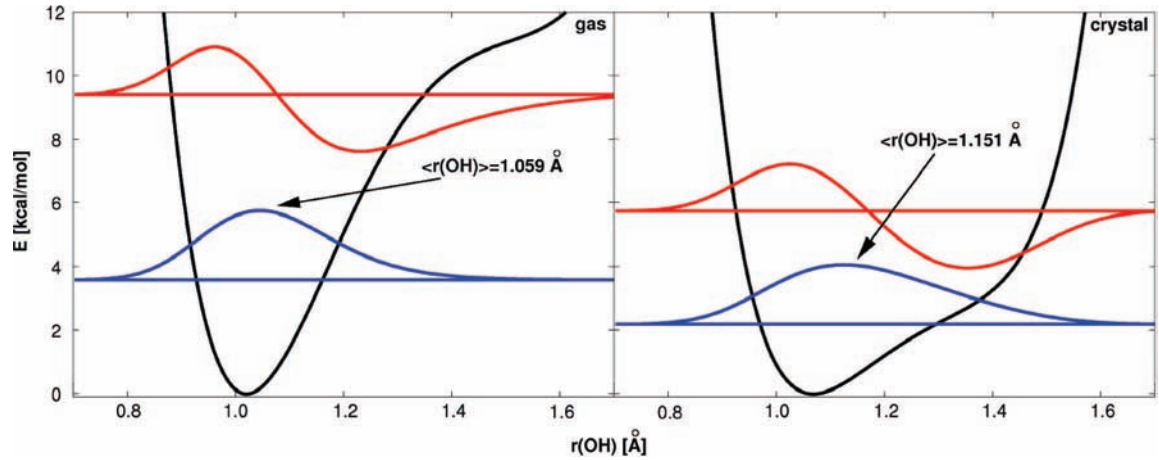

Figure 10. Proton potential (black line) together with the corresponding ground (blue line) and first excited (red line) vibrational levels and wavefunctions of TAE calculated with the gas phase model (left) and crystal field model (right). The ground state expectation value of the OH distance is also displayed.

O2 site. This does not necessarily imply that the resulting long-time average structure is symmetric with the proton equally distant from O1 and O2, because the crystal field can still render the O1 and O2 sites to be inequivalent. Additionally, the tendency of the proton to migrate from O2 to O1 is likely to be considerably overestimated due to the underestimated energy barrier, a well known feature common to DFT methods. Because of the need of long MD simulations coupled with the inevitable artifacts of DFT which lower the proton transfer barrier, we did not pursue further MD treatment of TAE.

The common feature of both proton potentials (Figure 10) is that they are asymmetric and have only one minimum closer to O2. The degree of asymmetry of both potentials is significant and originates from the fact that the geometry was kept frozen during the pointwise elongation of the O−H bond. Both potentials are, however, consistent with the asymmetric location of the proton, determined by neutron diffraction, where the gas phase potential energy surface gives a more confined area for the proton motion than the crystal potential. In the latter a relatively wide, low energy space range is accessible for the proton even at low temperatures which does suggest that the proton can migrate to the acceptor site. We reiterate that the proton dynamics in short hydrogen bonds is rather complicated because of coupling to other internal degrees of freedom and to the crystal field; any one-dimensional projection must therefore be viewed as a somewhat crude simplification. Nonetheless, the qualitative agreement between TAE potentials displayed on Figure 10, especially the one calculated with the crystal field model, as well as the observed location of the proton, provides some further justification for the present strategy of potential energy calculations, namely that single point scans are more appropriate than relaxed scans for the reproduction of a number of properties of hydrogen bonds.[34,35,58] From a structural point of view, the flat asymmetric potential obtained in the crystal model is reasonable and potentially useful for calculations of other properties of TAE.

Conclusions

Results obtained from our variable temperature neutron diffraction study demonstrate that the H1 proton involved in the short, intramolecular hydrogen bond of TAE is more centered between the donor and acceptor oxygen atoms at room temperature, and migrates closer to the oxygen atom to which it is covalently bound, at lower temperature. Periodic density functional quantum calculations using a periodic crystal field reproduce the hydrogen bond geometry well, particularly at low temperatures, but less so at room temperature. The tendency of the proton to migrate toward the center of the hydrogen bond with increasing temperature may be explained through the increased vibrational amplitude of the proton, effectively simulated by molecular dynamics. The single point energy scan reasonably reproduces the asymmetric character of the hydrogen bond of TAE.

Dynamic disorder in terms of a superposition of tautomers of TAE is found at 298 K, but this disorder is not present at 110 K and below, which confirms results reported in 2003 from an X-ray study of the compound.[13] In contrast to the earlier work, we find from the charge density analysis that the O−H···O bond has a significant shared interaction at 20 K. The removal of the dynamic disorder is in fact most likely the result of short intermolecular C−H···O contacts. Topological analysis of these short contacts reveals that there is a significant closed-shell interaction that influences the crystal structure. The hydrogen bond is found to have both covalent and electrostatic character, as was found in the 1998 study on benzoylacetone,[6] although the degree of delocalization is not as strong in TAE. Although TAE is a symmetrically substituted β-diketone enol, and hence should exhibit strong RAHB because of PA/pK_a matching,[15] it is most likely that the encroachment of neighboring molecules in the crystal mitigates this tendency, resulting in the asymmetric structure.

Acknowledgment. P.M.B.P. is grateful to Drs. V. V. Zhurov, Y.-S. Chen and E. Yearley for valuable experimental assistance with the charge density measurements. Work at Argonne National Laboratory was supported by the U.S. Department of Energy, Office of Science, Office of Basic Energy Sciences, under contract DE-AC02-06CH11357. Financial support from the Slovenian Ministry of Higher Education, Science and Technology (grant P1-0012) is gratefully acknowledged.

Supporting Information Available: CCDC 668912-668914, 671251 and 673379 contain the supplementary neutron crystallographic data for this paper. These data can be obtained free of charge from The Cambridge Crystallographic Data Centre via www.ccdc.cam.ac.uk/data_request/cif. All crystallographic data and a complete citation for ref 31. This material is available free of charge via the Internet at http://pubs.acs.org.

References and Notes

(1) Wilson, C. C. *C. R. Chimie* **2005**, *8*, 1434.
(2) Cowan, J. A.; Howard, J. A. K.; McIntyre, G. J.; Lo, S. M. F.; Williams, I. D. *Acta Crystallogr.* **2003**, *B59*, 794.
(3) Steiner, T.; Majerz, I.; Wilson, C. C. *Angew. Chem. Int. Ed.* **2001**, *40*, 2651.
(4) Wilson, C. C. *Acta Crystallogr.* **2001**, *B57*, 435.
(5) Gilli, G.; Bellucci, F.; Ferretti, V.; Bertolasi, V. *J. Am. Chem. Soc.* **1989**, *111*, 1023.
(6) Madsen, G. K. H.; Iversen, B. B.; Larsen, F. K.; Kapon, M.; Reisner, G. M.; Herbstein, F. H. *J. Am. Chem. Soc.* **1998**, *120*, 10040.
(7) Herbstein, F. H.; Iversen, B. B.; Kapon, M.; Larsen, F. K.; Madsen, G. K. H.; Reisner, G. M. *Acta Crystallogr., Sect. B* **1999**, *55*, 767.
(8) Jeffrey, G. A. *An Introduction to Hydrogen Bonding*; Oxford University Press: New York, 1991.
(9) Pakiari, A. H.; Eskandari, K. *J. Mol. Struct. (THEOCHEM)* **2006**, *759*, 51.
(10) Power, L. F.; Turner, K. E. *J. Cryst. Mol. Struct.* **1975**, *5*, 59.
(11) Seliger, J. ; Hadži, D. to be published.
(12) Tayyari, S. F.; Zahedi-Tabrizi, M.; Laleh, S.; Moosavi-Tekyeh, Z.; Rahemi, H.; Wang, Y. A. *J. Mol. Struct.* **2007**, *827*, 176.
(13) Lyssenko, K. A.; Lyubetsky, D. V.; Antipin, M. Y. *Mendeleev Commun.* **2003**, *2*, 60.
(14) Gilli, G.; Gilli, P. *J. Mol. Struct.* **2000**, *552*, 1.
(15) Gilli, P.; Bertolasi, V.; Pretto, L.; Ferretti, V.; Gilli, G. *J. Am. Chem. Soc.* **2004**, *126*, 3845.
(16) Schultz, A. J.; De Lurgio, P. M.; Hammonds, J. P.; Mikkelson, D. J.; Mikkelson, R. L.; Miller, M. E.; Naday, I.; Peterson, P. F.; Porter, R. R.; Worlton, T. G. *Physica B* **2006**, *385*, 386–1059.
(17) Schultz, A. J.; Carlin, R. L. *Acta Crystallogr., Sect. B* **1995**, *51*, 43.
(18) Jacobson, R. A. *J. Appl. Crystallogr.* **1976**, *19*, 283.
(19) Sears, V. F. In *Neutron Scattering*; Methods of Experimental Physics; Academic Press: Orlando, FL, 1986; Vol. 23, Part A.
(20) Howard, J. A. K.; Johnson, O.; Schultz, A. J.; Stringer, A. M. *J. Appl. Crystallogr.* **1987**, *20*, 120.
(21) Larson, A. C.; Von Dreele, R. B. General Structure Analysis System−GSAS; Los Alamos National Laboratory, 2000.
(22) Zhurov, V. V.; Zhurova, E. A.; Chen, Y.-S.; Pinkerton, A. A. *J. Appl. Cryst.* **2005**, *38*, 827.
(23) Zhurova, E. A.; Zhurov, V. V.; Tanaka, K. *Acta Crystallogr. Sect. B* **1999**, *55*, 917.
(24) Otwinowski, Z.;Zhurov, V. V. *Methods in Enzymology, Vol. 276, Macromolecular Crystallography*, Part A; Carter, C. W., Jr., Sweet, R. M., Eds.; Academic Press: New York, 1997; pp. 307–326.
(25) Blessing, R. H. *Cryst. Rev.* **1987**, *1*, 3.
(26) Sheldrick, G. M. SHELXTL, version 5.0 ed.; Bruker AXS Inc.: Madison, WI, 2001.
(27) Stewart, R. F. J. *J. Phys. Chem.* **1973**, *58*, 1668.
(28) Hansen, N. K.; Coppens, P. *Acta Crystallogr., Sect. A* **1978**, *34*, 904.
(29) Koritsanzky, T. ; Howard, S. T.; Mallinson, P. R.; Su, Z.; Richter, T.; Hansen, N. K. *XD Program, a Computer Program Package for Multipole Refinement and Analysis of Charge Densities from Diffraction Data*; Freie Universitat: Berlin, Germany, 1995.
(30) Saunders, V. R.; Dovesi, R.; Roetti, C.; Causa, M.; Harrison, N. M.; Orlando, R.; Zikovich-Wilson, C. M. *CRYSTAL 98 User's Manual*; Universita di Torino: Torino, Italy, 1998.
(31) Frisch, M. J.; et al. *Gaussian 03*, revision B.03; Gaussian, Inc.: Pittsburgh, PA, 2003.
(32) Car-Parrinello Molecular Dynamics, version 3.9.2; IBM Corp., 1990−2004.
(33) Laasonen, K.; Pasquarello, A.; Lee, C.; Car, R.; Vanderbilt, D. *Phys. Rev. B* **1993**, *47*, 10142.
(34) Babić, D.; Bosanac, S. D.; Došlić, N. *Chem. Phys. Lett* **2002**, *358*, 337.
(35) Panek, J.; Stare, J.; Hadži, D. *J. Phys. Chem. A* **2004**, *108*, 7417.
(36) Balint-Kurti, G. G.; Dixon, R. N.; Marston, C. C. *Int. Rev. Phys. Chem.* **1992**, *11*, 317.
(37) Stare, J.; Balint-Kurti, G. G. *J. Phys. Chem. A* **2003**, *107*, 7204.
(38) Wilson, C. C. *Single Crystal Neutron Diffraction from Molecular Materials*; World Scientific Publishing Co. Pte. Ltd: Singapore, 2000.
(39) Lyssenko, K. A.; Antipin, M. Y. *Russ. Chem. Bull., Int. Ed.* **2006**, *55*, 1.
(40) Hirschfeld, F. L. *Acta Crystallogr., Sect. A* **1976**, *32*, 239.
(41) Maverick, E. F.; Trueblood, K. N. *Thermal Motion Analysis Program THMA-11 Zurich* **1987**,
(42) Bondi, A. *J. Phys. Chem.* **1964**, *68*, 441.
(43) Spackman, M. A.; Byrom, P. G. *Chem. Phys. Lett.* **1997**, *267*, 215.
(44) McKinnon, J. J.; Mitchell, A. S.; Spackman, M. A. *Chem.-Eur. J.* **1998**, *4*, 2136.
(45) Allen, F. H. *Acta. Crystallogr. Sect. B* **2002**, *58*, 380.
(46) Wolff, S. K.; Grimwood, D. J.; McKinnon, J. J.; Jayatilaka, D.; Spackman, M. A. CrystalExplorer 2.0; University of Western Australia: Perth, 2006.
(47) Madsen, G. K. H.; Wilson, C.; Nymand, T. M.; McIntyre, G. J.; Larsen, F. K. *J. Phys. Chem. A* **1999**, *103*, 8684.
(48) Bader, R. F. W. *Atoms in Molecules. A Quantum Theory*; Clarendon Press: Oxford Science Publications: Oxford, U.K., 1990.
(49) Gatti, C. *Z. Kristallogr.* **2005**, *220*, 399.
(50) Coppens, P. *X-Ray Charge Density and Chemical Bonding*; Oxford University Press: Oxford, U.K., 1997.
(51) Bader, R. F. W. *J. Phys. Chem. A* **1998**, *102*, 7314.
(52) Espinosa, E.; Alkorta, I.; Elguero, J.; Molins, E. *J. Chem. Phys.* **2002**, *117*, 5529.
(53) Roversi, P.; Brazaghi, M.; Merati, F.; Destro, R. *Can. J. Chem.* **1996**, *74*, 1145.
(54) Wilson, C. C.; Morrison, C. A. *Chem. Phys. Lett.* **2002**, *362*, 85.
(55) Fontaine-Vive, F.; Johnson, M. R.; Kearley, G. J.; Howard, J. A. K.; Parker, S. F. *J. Am. Chem. Soc.* **2006**, *128*, 2963.
(56) Stare, J. ; Panek, J. ; Eckert, J. ; Grdadolnik, J. ; Mavri, J. ; Hadži, D. *J. Phys. Chem. A* **1998**, *112*, 1576.
(57) Morrison, C. A.; Siddick, M. M.; Camp, P. J.; Wilson, C. C. *J. Am. Chem. Soc.* **2005**, *127*, 4042.
(58) Demšar, K. ; Stare, J. ; Mavri, J. *J. Mol. Struct.* **2007**, *844*, 215.

JP800204R